SCIENCE CHINA

Technological Sciences

December 2010 Vol.53 No.12: 3175–3182 doi: 10.1007/s11431-010-4173-3

Ab initio molecular dynamics simulation of the atom packing and density of Al-Ni amorphous alloys

YU ChunYan¹, HUI XiDong^{1*}, CHEN XiaoHua¹, LIU XingJun¹, LIN DeYe¹, LIU ZiKui² & CHEN GuoLiang¹

¹ State Key Laboratory for Advanced Metals and Materials, University of Science and Technology Beijing, Beijing 100083, China; ² Department of Materials Science and Engineering, Pennsylvania State University, University Park, PA 16802, USA

Received June 18, 2010; accepted September 16, 2010

Al-Ni alloys have better glass forming ability (GFA) than other Al-based alloys. However, the relationship among the atomic arrangement, glass transition, packing density and composition hasn't been systematically studied. In this paper the *ab initio* molecular dynamics simulation (AIMD) was performed on the atom packing and density of $Al_xNi_{100-x}(x=80, 83, 85, 86, 87)$ and 90) alloys. The pair correlation function and Voronoi tessellation indicated that there are obvious topological and chemical short-range orders in these alloys. The topological structure consists of Al-centered icosahedra like and Ni-centered tri-capped trigonal prism (TTP) like polyhedra. There is strong chemical short-range ordering between Al and Ni atoms indicated by the bond-length of Al-Ni pair shorter than the sum of the radii of Al and Ni atoms, which increases with the increasing of Ni content. It is shown that the densities of amorphous alloys don't agree with the linear law with a peak at x=85. Based on the features of the structure and density, it is concluded that Al-Ni alloys at x=84-86 have high GFA, which can be extended to multi-component Al-based alloys.

AIMD, Al-Ni alloys, density, short-range order, chemical short-range order

itation: Yu C Y, Hui X D, Chen X H, et al. *Ab initio* molecular dynamics simulation of the atom packing and density of Al-Ni amorphous alloys. Sci China Tech Sci, 2010, 53: 3175–3182, doi: 10.1007/s11431-010-4173-3

1 Introduction

Al-based amorphous alloys have always been attracting great interest due to its high strength, low density, good corrosion resistance and wear resistance. In the 1980s, metallic glasses with good toughness and corrosion resistance were prepared in Al-EM (early transition metal)-LM(late transition metal) [1], Al-Re(rare earth metal)-LM [2], and Al-TM-Re [3] systems. However, for most of the systems, only amorphous ribbons and powders have been prepared because of the poor glass forming ability (GFA), which largely restricts their applications. In order to improve their

GFA, researches involving thermodynamics [4], kinetics [5], atomic size mismatch [6], chemical reaction [7], and atomic structure [8] have been performed. To understand the nature and mechanism of glass formation, and acquire valuable information for composition design with high GFA, it is of great significance to characterize the atomic structure of liquid and amorphous alloys, and the structural evolution during the glass transition.

The structural features of liquid and glassy Al-Mn [9], Al-Fe [10], Al-Fe-Ce [11], Al-Y [12], Al-Y-Ni [12] and Al-Ni [13, 14] systems have been investigated by using X-ray diffraction and neutron diffraction and so on. These experiments have provided some useful information to understand the structure of Al-based glasses, but the results derived from these experiments only reflected the statistical

^{*}Corresponding author (email: xdhui@ustb.edu.cn)

average information. To understand the local order structure, rational theoretical structure modeling should be introduced. Recently, the investigation of the structure of liquid and metallic glasses by using ab initio molecular dynamics (AIMD) simulation and reverse Monte Carlo (RMC) simulation has attracted more and more attention. Jakse et al. calculated the structure of Al₈₀Mn₂₀ alloy by using AIMD and RMC methods, and found the Mn-centred five-folded structural characteristics [15, 16]. Bian et al. [17, 18] systematically investigated the Al-Fe alloys by classical molecular dynamic (MD) and AIMD simulation, and found that the bonding between EM transition elements and Al or Fe atoms has a significant effect on their GFA. As Al-Ni system has better GFA than other Al-based alloys [19, 20], calculations have been performed on the short-range order (SRO) of Al₈₀Ni₂₀ [15, 21, 22], Al-Ni-Y [23], Al₈₉La₆Ni₅ [24, 25], etc. However, universal recognition of the relationship among the atomic arrangement, glass transition, packing density and composition hasn't been attained till now. More importantly, either the early random dense packing hard sphere model [26] or the dense packing cluster model and the quasi-equivalent clusters stacking model proposed by Miracle [27] and Sheng [28], respectively is related to the atomic dense packing, but theoretical or quantitative experimental data were not given in these models. Recently, Li et al. [29] measured the expansion coefficient of Cu-Zr binary glassy alloys. They found that the densities were abnormally high for certain composition with high GFA. This result indicates that the variation of density with composition has implication to understanding the essence of GFA. In this paper, AIMD simulation was performed on Al_xNi_{100-x} (x = 80, 83, 85, 86, 87, 90) binary alloys to study the liquid-solid transition, and the variation of atomic structure and packing density with composition. The correlation among these three parameters was clarified, which is expected to provide a theoretical basis for the composition design of Al-based alloys with high GFA.

2 Methodology

The *ab initio* molecular dynamics (AIMD) simulation is based on density-function theory (DFT) which was firstly proposed by Car and Parrinello in 1985 [30]. This simulation method does not need to know the accurate interaction potential between elements as the classical molecular dy-

namics simulation did. Our calculation was performed by using Viena ab initio simulation program (VASP) [31, 32]. A cubic supercell with 200 atoms was constructed as the initial configuration. Al and Ni atoms were distributed randomly in the cubic supercell with the initial density obtained by mass/average atomic volume. At each temperature platform, the supercell volume was adjusted corresponding to zero external pressure, as known of "zero external pressure" method, the relative position of atoms was fixed in this process. Projector augmented wave (PAW) [33, 34] potential was adopted to describe the coulomb interaction of ion core on the valence electrons. The electronic exchange and correlation were described in the generalized gradient approximation (GGA) [35]. The simulation was performed in a canonical ensemble with a Nose'thermostat [36] for temperature control. The equation of motion was solved via the velocity Verlet algorithm [37] with a time step of 5 frame/s.

The cooling routes adopted for every alloy in the simulation were shown in Figure 1. For each alloy, the system was firstly equilibrated for 3000 steps at 2000 K to obtain equilibrating configuration out of the impact of initial configuration. Then the system was equilibrated sequentially at $1.3T_{\rm L}$ ($T_{\rm L}$ is the liquidus temperature in thermodynamic equilibrium phase diagram, as listed in Table 1) for 3000 steps, to acquire equilibrium configurations and kinetic properties at this temperature. Finally, the system was quenched to 300 K with a cooling rate of 5×10^{13} K/s, and kept at this temperature for 1000 steps to get the ultimate amorphous configuration.

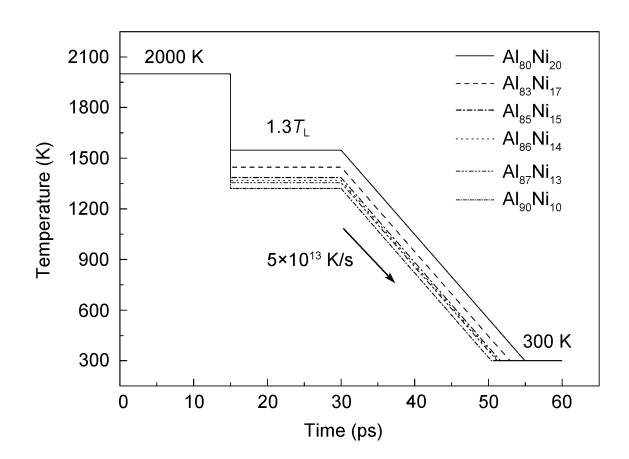


Figure 1 Schematic of the quenching process for Al_xNi_{100-x} alloys.

Table 1 Liquidus temperature, T_L and the initial density, ρ employed in the simulation

Alloys	$Al_{80}Ni_{20}$	$Al_{83}Ni_{17}$	$Al_{85}Ni_{15}$	$Al_{86}Ni_{14} \\$	$Al_{87}Ni_{13}$	$Al_{90}Ni_{10}$
$T_{L}\left(\mathbf{K}\right)$	1253	1176	1125	1116	1109	1078
$1.3T_{\rm L}\left({ m K}\right)$	1629	1529	1463	1451	1442	1401
ρ (Å ⁻³)	0.06464	0.06394	0.06348	0.06326	0.06303	0.06236

3 Results and discussion

3.1 Pair correlation functions

The pair correlation function (PCF) is one of the main parameters which are used to reveal the structural characteristics of liquid and amorphous states. It can be derived from the Fourier transformation of the structure factors. The partial pair correlation function $g_{ij}(r)$ is defined by the probability of finding particle j in the spherical shell where particle i is taken as the center, i.e., [38]

$$g_{ij}(r) = \frac{L^3}{N_i N_j} \left\langle \sum_{i=1}^{N_i} \frac{n_{ij}(r, \Delta r)}{4\pi r^2 \Delta r} \right\rangle, \tag{1}$$

where L denotes the length of the cubic supercell; N_i and N_j are the numbers of ions of i and j species, respectively, and $n_{ij}(r,\Delta r)$ is the number of ions of j species in the sphere shell from r to $r+\Delta r$, as referenced to i species. There are n(n+1)/2 different partial PCFs in a system with n kinds of species, the generalized PCF was obtained by the linear combination of the partial PCFs [39], i.e.,

$$g(r) = \sum_{i} \sum_{j} c_{i} c_{j} \frac{f_{i}(Q) f_{j}(Q)}{\langle f(Q) \rangle^{2}} g_{ij}(r), \qquad (2)$$

where $\langle f(Q) \rangle^2 = \left(\sum c_i f_i(Q)\right)^2$, $i=1, 2, 3, \dots, n$; c_i and c_j are the concentrations of i and j species, respectively, $f_i(Q)$ and $f_j(Q)$ are the neutron scattering coefficients of i and j species, respectively. The structure factor is then obtained from the Fourier transformation of its PCF, g(r), by the equation [38]:

$$S(Q) = 1 + \rho_0 \int_0^\infty 4\pi r [g(r) - 1] \frac{\sin(Qr)}{Q} dr.$$
 (3)

The reduced atomic distribution function G(r) [40] is defined as

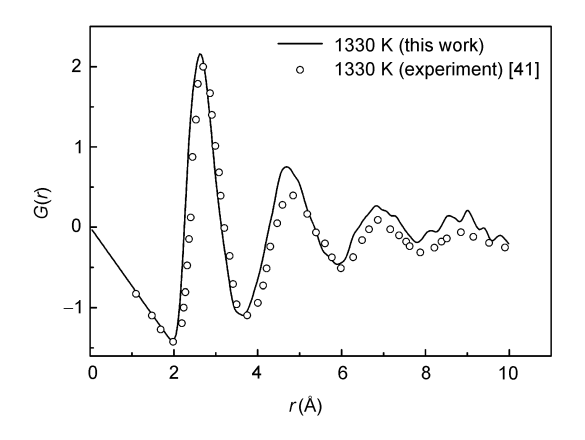
$$G(r) = 4\pi r^2 \rho_0(r)(g(r) - 1), \tag{4}$$

where $\rho_0(r)$ is the average atomic density.

Figure 2 shows the comparison of the simulation results of S(Q) and G(r) with the experiment results [41] for liquid $Al_{80}Ni_{20}$ alloy at 1330 K. It can be seen that AIMD simulation results agreed with the experiment results very well. Our AIMD simulation nearly reproduced the shapes and positions of the experimentally measured PCF peaks, although there was a slight difference in the heights of the peaks. This difference didn't influence the correctness of our simulation. The reason for this situation was the fact that there were many factors, e.g., scattering coefficients and specimen size, influencing the scattering intensity in experiments.

The partial PCFs of heterogenic atomic pairs and homogenic atomic pairs and the generalized PCF of liquid and amorphous Al-Ni alloys, $g_{\text{Al-Al}}(r)$, $g_{\text{Al-Ni}}(r)$, $g_{\text{Ni-Ni}}(r)$ and g(r) were shown in Figure 3. Some features of the PCFs for these Al-Ni alloys could be observed. After quenched into the glass state, all the heights of the first peaks became higher, and the positions shifted to the right-hand side slightly. The second peaks of $g_{\text{Al-Ni}}(r)$, $g_{\text{Al-Ni}}(r)$ and $g_{\text{Ni-Ni}}(r)$ exhibited pronounced splitting, indicating the development of short-range order in the structure.

The second peaks of $g_{Al-Al}(r)$ of all the six alloys occurred splitting evidently, reflecting obvious short-range ordering of Al-Al atom pairs. What is more, the right splitting sub-peak of the second peak increased with the increase of Al content. When the Al content was 86%, 87% and 90%, the two splitting sub-peaks were nearly the same high. Compared to $g_{Al-Al}(r)$, the peaks of $g_{Al-Ni}(r)$ were higher and narrower, revealing stronger interaction between Al-Ni than Al-Al. Except for the two alloys with x=80, 83, the second peaks of $g_{Al-Ni}(r)$ all split, whereas the variation of splitting with the Al content could not be seen. It was noticed that the first peaks of $g_{Ni-Ni}(r)$ were much lower than the second peaks, indicating strong interaction between Al and Ni species. The dominant species in the first shell of Ni was Al, while the Ni atoms occupied the second shell. We could also see splitting on the second peak of $g_{Ni-Ni}(r)$ curves of all



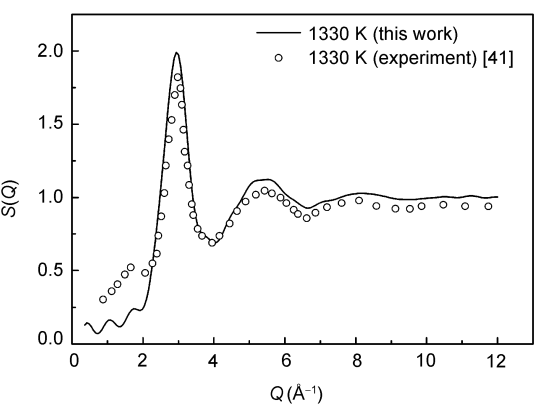


Figure 2 Comparison of the liquid G(r) and S(Q) of $Al_{80}Ni_{20}$ binary alloy from the AIMD calculation with the experimental data [41].

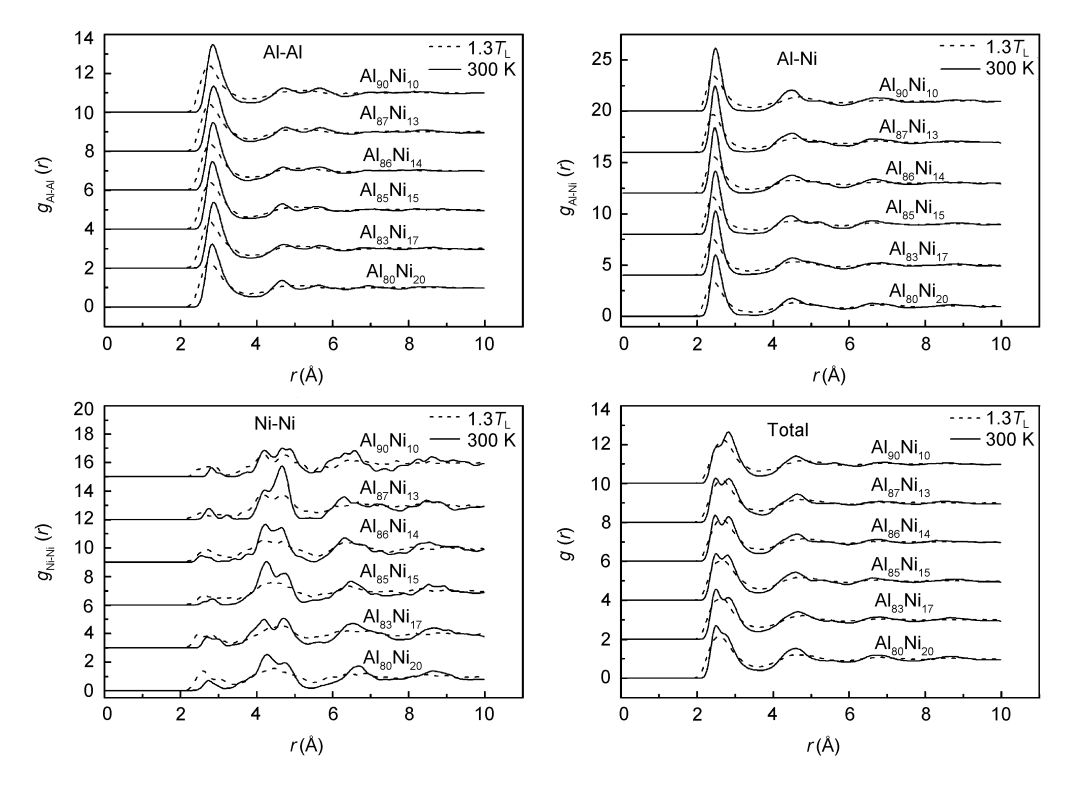


Figure 3 Pair correlation functions in liquid (dashed lines) and amorphous (solid lines) Al_xNi_{100-x} alloys.

the six alloys, and the intensity of the right sub-peak tended to increase firstly and then to decrease with the increase of Al content. The second peaks of $g_{\text{Ni-Ni}}(r)$ were the highest among all the peaks at x=85, 86 and 87. Obvious splitting in the first peaks of general g(r) was observed because of large radius difference between Al and Ni atoms. The first peak became wider, while the right sub-peak of it became higher and sharper with the increase of Al content. Slight splitting occurred on the second peaks of general g(r), which wasn't obviously affected by the content of Al.

3.2 Voronoi tessellation and coordination number

In the following sections, we will present the geometric features of atomic clusters by using the Voronoi tessellation method which was developed by Finney in 1970 [42]. The Voronoi polyhedron is defined as the smallest closed convex polyhedron formed by the perpendicular bisector surfaces of the lines connecting the central atom and the adjacent atoms, reflecting the local nearest-neighbor coordination, described by the Voronoi index $\langle n_3, n_4, n_5, n_6, \cdots \rangle$, where n_i denotes the number of *i*-edged faces of the Voronoi polyhedron and Σn_i is the total coordination number (CN). The type of the coordination polyhedron with a certain central atom can be identified through the Voronoi index. For example, $\langle 0, 12, 0, 0 \rangle$ represents face-centered cubic (fcc) structure with CN=12; (0, 6, 0, 8) body-centered cubic (bcc) structure with CN=14; $\langle 0, 0, 12, 0 \rangle$ icosahedral structure with CN=12.

The distributions of Voronoi polyhedrons of all the six alloys were calculated. It was seen that the polydradrons with Z9 <0, 3, 6, 0> were the highest, while the average CN=12 and 13 of all the atoms in the six kinds of alloys were dominant. It can be easily understood that there were many types of polyhedra appearing such as (0, 3, 6, 3), (0, 2, 3, 6, 3)8, 2, (0, 3, 6, 4), (0, 1, 10, 2) with the CN=12 and 13, but only one kind of polyhedron (0, 3, 6, 0) appeared with CN=9. Taking the Al₈₅Ni₁₅ alloy for example (as shown in Figure 4), Z9 (0, 3, 6, 0) was dominant in the Voronoi distribution, with the highest percentage 7%. However, the frequency of CN=9 in Al₈₅Ni₁₅ glass was only about 10%, while CN=12 and 13 occupies 26.01% and 29.67%, respectively, corresponding to the polyhedra Z12 (0, 3, 6, 3), Z12 (0, 2, 8, 2), Z13 (0, 3, 6, 4) and Z13(0, 1, 10, 2). Similar results in other five alloys could also be obtained. It was seen that the Voronoi polyhedra with five-edged faces were dominant, indicating that the SROs exhibited the feature of five-folded symmetry, which is true even for the polyhedra with frequencies lower than 2%.

The Voronoi polyhedron and CN distributions with the central atoms of Al and Ni respectively were shown in Figure 5. The CN of the Al-centred Voronoi polyhedra ranged from 9 to 16, CN=12 and 13 were dominant. As for Ni-centred Voronoi polyhedral, CN ranged from 8 and 12 with CN=9 being dominant. There was a tendency for the variation of CN distribution with composition. It was seen that in the low CN range, the CN tended to increase with the increase of Al content, but in the high CN range, CN decreased.

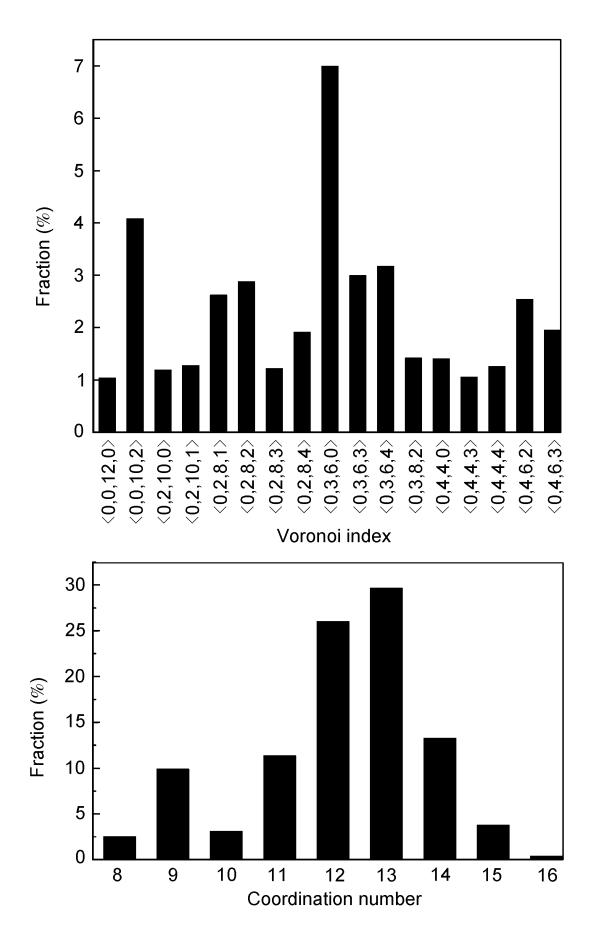


Figure 4 Voronoi polyhedra and CN distribution in $Al_{85}Ni_{15}$ amorphous allov.

It was shown that the Al-centered and Ni-centered polyhedra were completely different. There were a variety types of Al-centered polyhedra with the change of composition, among which $Z12\langle 0, 2, 8, 2 \rangle$, $\langle 0, 3, 6, 3 \rangle$ and $Z13\langle 0, 3, 6, 4 \rangle$, (0, 1, 10, 2) kept dominant. For example, the total fraction of these types of Al-centered polyhedra in Al₈₅Ni₁₅ was up to 65.4% (as shown in Figure 6). The Al-centred polyhedra were mainly composed of defective icosahedra and Frank-Kasper polyhedra [43] with CN between 14 and 16. It is to say that the Al atoms are in the coordination circumstance similar to icosahedron. The CNs of Ni-centered polyhedra in the six alloys were all less than 12. <0, 3, 6, 0>, <0, 2, 8, 0> and <0, 4, 4, 0> which are related to Bernal polyhedra [44] were the dominant polyhedra (here, $\langle 0, 3, 6, 4 \rangle$ 0) represents tri-capped trigonal prism packing(TTP [8]), (0, 3, 6, 1) is the TTP counterpart; (0, 2, 8, 0) the bi-capped square archimedean antiprism(BASP) [8], <0, 2, 8, 1> is the BASP counterpart; (0, 4, 4, 0) the standard square dodecahedron). The Z8 $\langle 0, 4, 4, 0 \rangle$ and Z9 $\langle 0, 3, 6, 0 \rangle$ polyhedra tended to increase firstly and decrease sequentially with the increase of Al content. The Z9 polyhedron of Al₈₅Ni₁₅ was the highest of all the six alloys, reaching up to 64.9%. The fractions of Z10 $\langle 0, 2, 8, 0 \rangle$, $\langle 0, 3, 6, 1 \rangle$ and Z11 $\langle 0, 2, 8, 1 \rangle$

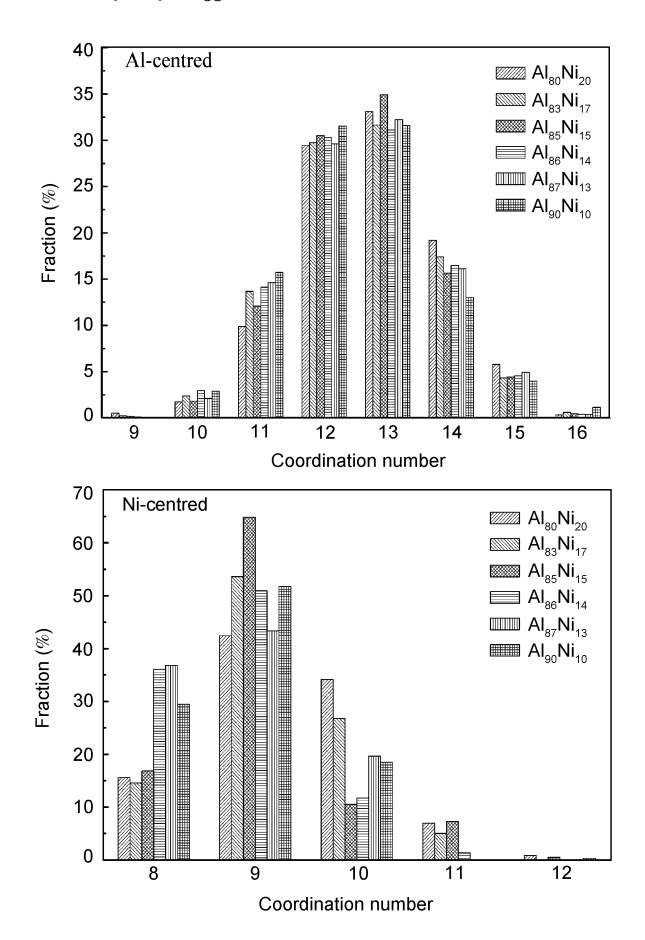


Figure 5 The Al-centred and Ni-centred CN distribution in Al_xNi_{100-x} amorphous alloys.

polyhedra decreased with the increase of Al content. In binary systems, it has been proven that the preference for a particular type polyhedron is controlled by the effective atomic size ratio of the solute to solvent atoms, R^* . With decreasing R^* , the preferred polyhedra type changes from the Frank-Kasper type (for $R^* > 1.2$) to the icosahedral type ($R^* < 0.902$), and then to the BSAP type ($R^* < 0.835$), and finally to the TTP type ($R^* < 0.732$) [8]. As for Al-Ni binary system, $0.835 < R_{\rm Ni}/R_{\rm Al} < 0.902$, but the dominant polyhedron in the Ni-centered polyhedra is of TTP type, not icosahedral or BASP type. Ni is located in a coordination environment similar to the crystal structure, implying that the SRO depends on not only the atomic radius size ratio of the two species but also the chemical interaction.

Icosahedra exist extensively in metallic glasses as a dense packing structure. It is generally accepted that the high concentration of icosahedra reflects high GFA of an alloy. Figure 6 showed that icosahedron Z12 $\langle 0, 0, 12, 0 \rangle$ were all centred by Al atoms, of which the concentration was much lower than that of other types of polyhedra. This may be one of the reasons for the low GFA of Al-based glasses. Table 2 showed the fractions Z12 $\langle 0, 0, 12, 0 \rangle$ in all the interested alloys. It was found that the number of Z12 increased from liquid to amorphous state, and was the highest

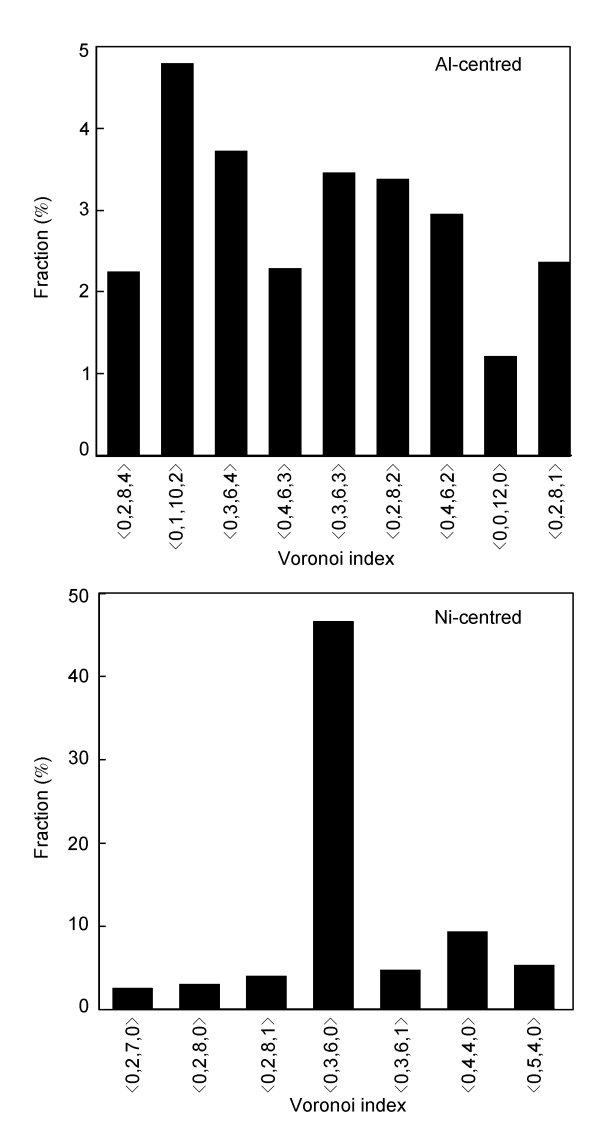


Figure 6 The Al-centred and Ni-centred voronoi polyhedra distribution in $Al_{85}Ni_{15}$ amorphous alloy.

in Al₈₆Ni₁₄ glassy alloy. If the concentration of Z12<0, 0, 12, 0> is the only criterion to judge the GFA, it is the Al₈₆Ni₁₄.

3.3 Chemical short range order

We have discussed the topological short-range order (TSRO) in Al-Ni binary amorphous alloys. Here we will focus on the chemical short-range order (CSRO) in them. It has been proven that CSRO exists extensively in Al-based metallic glasses [14, 45, 46]. The intensity of the first peak of PCF reflects the chemical interaction between different species qualitatively. It was seen in Figure 3 that at room temperature, the intensity of the first peak of $g_{\text{Al-Ni}}$ was higher than that of $g_{\text{Al-Al}}$ and $g_{\text{Ni-Ni}}$, indicating that the chemical interaction between heterogeneous species was stronger than that between homogeneous species. Table 3 showed the calculated partial atomic nearest distances and CNs, which were acquired from integration under the first peaks of PCFs, expressed as [40]

$$N_{m} = \int_{r_{0}}^{r_{\min}} 4\pi \rho_{0} r^{2} g(r) dr.$$
 (5)

From Table 3, it was seen that the nearest displacement between Al and Al atoms was nearly the same as the sum of their atomic radii, whereas that of Ni-Ni was much lager than the sum of atomic radii. For Al-Ni pair, the nearest displacement was 2.48, much smaller than their sum of atomic radii, indicating strong interaction between Al and Ni species. We also calculated the Warren-Cowley CSRO parameter α_{ij} [47] to characterize the chemical interaction. The α_{ij} is defined as

$$\alpha_{ij} = 1 - N_{ij} / c_j (N_{ij} + N_{ii}),$$
 (6)

where *i* represents Ni species, N_{ij} and N_{ii} are the partial CN around Ni, and c_j is the mole fraction of Al. The calculated results were also shown in Table 3. It was seen that the α_{NiAl}

 $\textbf{Table 2} \quad \text{The fraction of voronoi polyhedron } \langle 0, 0, 12, 0 \rangle \text{ in liquid and amorphous } Al_xNi_{100-x} \text{ alloys}$

	$Al_{80}Ni_{20}$	$Al_{83}Ni_{17}$	$Al_{85}Ni_{15}$	$Al_{86}Ni_{14} \\$	$Al_{87}Ni_{13}$	$Al_{90}Ni_{10}$
$1.3T_{ m L}$	0.635	0.575	0.975	0.7	1.115	0.85
300 K	0.97	0.825	1.035	1.935	0.825	1.65

Table 3 Structural parameters of Al_xNi_{100-x} amorphous alloys from the AIMD calculation (partial atomic nearest distance R_{ij} , partial coordination number N_{ij} , chemical short-range order parameter α_{ij})

Alloys	$r_{ m Al-Al}$	$r_{ m Al-Ni}$	$r_{ m Ni-Ni}$	$N_{ m Al-Al}$	$N_{ m Al-Ni}$	$N_{ m Ni ext{-}Al}$	$N_{ m Ni-Ni}$	$lpha_{ m NiAl}$
x=80	2.82	2.48	2.72	11.03	2.21	8.85	0.32	-0.206
<i>x</i> =83	2.88	2.48	2.72	11.04	1.75	8.57	0.38	-0.154
x=85	2.85	2.48	2.85	10.69	1.55	8.77	0.13	-0.159
x=86	2.85	2.48	2.55	10.89	1.37	8.41	0.13	-0.145
x=87	2.88	2.48	2.75	11.45	1.26	8.43	0.22	-0.120
<i>x</i> =90	2.85	2.48	2.82	11.64	0.97	8.74	0.10	-0.099

varied from -0.206 to -0.099 when the Al content increased from 80% to 90%, demonstrating strong chemical interaction between Al and Ni atoms. Moreover, this interaction tended to increase with the increase of Ni content. The strong bonding interaction might be attributed to the special outer electron structure (unfulfilled d or f orbit) of the transition elements in the alloys. They form stable hybrid orbits with Al atoms, which improve the bonding force among elements in the alloys [48]. However, as the Al content was 85%, this tendency seemed to be deviated, the absolute value of $\alpha_{\rm NiAl}$ was larger than those of ${\rm Al}_{84}{\rm Ni}_{16}$ and ${\rm Al}_{86}{\rm Ni}_{14}$. We speculated that there was stronger interaction between heterogeneous atoms, the atoms were more densely packed in ${\rm Al}_{85}{\rm Ni}_{15}$.

3.4 Atomic density

The GFA of amorphous alloys is always considered to be correlated to the packing density of atoms. Generally speaking, the higher the packing density, the closer the distance between atoms. Therefore, the free volume will be smaller and the viscosity may be larger, which results in better GFA. Either the random dense packing hard sphere model raised by Bernal [26], or the dense packing cluster packing model by Miracle [27], or the stacking model of quasi-equivalent clusters by Sheng [28], is based on this criterion. Experimentally, it is found that the density or mole volume has a great impact on GFA, concluding that the system with good GFA has smaller change of volume during the quenching or crystallization process [49, 50]. Li et al. [29] believed that the GFA is related to the amorphous density of a system. They evidenced that the alloys with good GFA show a peak in the density curve.

In this work, we tried to find some relationship between the amorphous density and GFA in Al-Ni alloy system. Figure 7 showed the amorphous density calculated from the "zero external pressure" method. It was seen that the amorphous density tended to decrease with the increase of Al content. This is easily understood that the radius of Al is larger than that of Ni. As x=85, there is a peak, which deviates from linear relationship obviously. This is similar to that phenomenon in Cu-Zr system found by Li et al. Therefore, we speculate that in the Al-based alloys with the Al content from 84% to 86%, the alloy has a higher atomic packing density. The high atomic packing density in the liquid state means high viscosities and the atoms move difficultly so that the liquid is more stable, and the nucleation and crystallization are inhibited.

Based on the results including PCFs, Voronoi tessellations, CSRO and densities, we speculate that as x=84–86, the GFA of this system is high. If we maintain the Al content within 84%–86%, and add other transition or RE elements into this system, the GFA will be improved largely. This has been proven to be valid in Al₈₅Ni₅Y₈Co₂ and Al₈₆Ni₉La₅ (of which the critical thicknesses reached

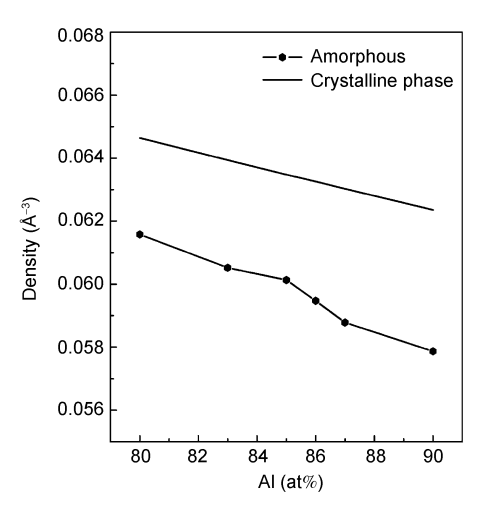


Figure 7 Atomic number density of Al_xNi_{100-x} amorphous alloy (The density of the crystalline phase was estimated from the equilibrium phase diagram using the lever rule).

900 μm [19] and 780 μm, respectively) [20].

4 Conclusions

- 1) The amorphous structure of Al_xNi_{100-x} alloys was characterized by employing AIMD simulation at a cooling rate of 5×10^{13} K/s. The PCFs indicate obvious SRO in this system. Voronoi tessellation shows that the SRO are mainly constituted by Al-centred icosahedral structure and Ni-centred TTP struture.
- 2) In Al-Ni binary amorphous alloys, the bond length of Al-Ni is less than their sum of radii, revealing that there are strong CSRO. This tendency increases with the increase of the content of Ni.
- 3) The densities of Al-Ni amorphous alloys were calculated based on the AIMD simulation results. It is shown that there is a peak at x=85. We speculate that $Al_{85}Ni_{15}$ has higher atomic packing density and higher stability of liquid than other alloys in this system.
- 4) Based on both the features of structure and density, we conclude that the GFA is high when the Al content is between 84% and 86%, which has been proven in the reported multi-component Al-Ni amorphous alloys.

This work was supported by the National Basic Research Program of China ("973" Program)(Grant No. 2007CB613901) and the National Natural Science Foundation of China (Grant Nos. 50871013, 50901006).

- Suzuki R O, Komatsu Y, Kobayashi K E, et al. Formation and crystallization of Al-Fe-Si amorphous alloys. J Mater Sci, 1983, 18(4): 1195–1201
- 2 Inoue A, Bizen Y, Kimura H M, et al. Development of compositional short-range ordering in an Al₅₀Ge₄₀Mn₁₀ amorphous alloy upon annealing. J Mater Sci Lett, 1987, 6(7): 811–814
- 3 He Y, Poon S J, Shiflet G J. Synthesis and properties of metallic

- glasses that contain aluminum. Science, 1988, 241(2): 1640-1642
- 4 Zhu A W, Shiflet G J, Miracle D B. Glass forming ranges of Al-rare earth metal alloys: Thermodynamic and kinetic analysis. Scripta Mater. 2004. 50(7): 987–991
- 5 Zhu A W, Poon S J, Shiflet G J. On glass formability of Al-Gd-Ni(Fe). Scripta Mater, 2004, 50(12): 1451–1455
- 6 Senkov O N, Miracle D B. Effect of the atomic size distribution on glass forming ability of amorphous metallic alloys. Mater Res Bull, 2001, 36(12): 2183–2198
- 7 Guo F Q, Enouf S, Poon S J. Formation of ductile Al based metallic glasses without rare-earth elements. Philos Mag Lett, 2001, 81(3): 203–211
- 8 Sheng H W, Luo W K, Alamgir F M, et al. Atomic packing and short-to-mediumrange order in metallic glasses. Nature, 2006, 439(26): 419–425
- 9 Inoue A, Masumoto T. X-ray diffraction study of amorphous Al_{77.5}Mn_{22.5} and Al₅₆Si₃₀Mn₁₄ alloys. J Mater Sci, 1988, 23(2): 753– 756
- 10 Zhang L, Wu Y S, Bian X F, et al. Short-range and medium-range order in liquid and amorphous Al₉₀Fe₅Ce₅ alloys. J Non-Cryst Solids, 2000, 262(1-3): 169–176
- 11 Qin J Y, Bian X F, Sliusarenko S I, et al. Pre-peak in the structure factor of liquid Al-Fe alloy. J Phys: Conden Matter, 1998, 10(6): 1211
- 12 Inoue A. Amorphous, nanoquasicrystalline and nanocrystalline alloys in Al-based systems. Prog in Mater Sci, 1998, 43(5): 365–520
- 13 Rachek O P. X-ray diffraction study of amorphous alloys Al-Ni-Ce-Sc with using Ehrenfests formula. J Non-Cryst Solid, 2006, 352(36-37): 3781–3786
- 14 Ahn K, Louca D, Poon S J, et al. Topological and chemical ordering induced by Ni and Nd in Al₈₇Ni₇Nd₆ metallic glass. Phys Rev B, 2004, 70(22): 224103
- Jakse N, le Bacq O, Pasturel A. Chemical and icosahedral short-range orders in liquid and undercooled Al₈₀Mn₂₀ and Al₈₀Ni₂₀ alloys: A first-principles-based approach. J Chem Phys, 2005, 123(10): 104508
- 16 Li R Y, Qin J Y, Gu T K, et al. Structure of liquid Al₈₀Mn₂₀ alloy by reverse Monte Carlo simulation. J Non-Cryst Solid, 2008, 354(15-16): 1736–1739
- 17 Li H, Ding F, Wang J L, et al. Structural studies of clusters in melt of FeAl compound. J Chem Phys, 2001, 114(14): 6413
- 18 Gu T K, Qin J Y, Bian X F. Correlation between local structure of melts and glass forming ability for Al-based alloys: A first-principles study. Appl Phys Lett, 2007, 91: 081907
- 19 Inoue A, Matsumoto N, Masumoto T. Al-Ni-Y-Co amorphous alloys with high mechanical strengths, wide supercooled liquid region and large glass forming capacity, Mater Trans-JIM, 1990, 31: 493–500
- 20 Sanders W S, Warner J S, Miracle D B. Stability of Al-rich glasses in the Al-La-Ni system. Intermetallics, 2006, 14: 348
- 21 Horbach J, Das S K, Griesche A, et al. Self-diffusion and interdiffusion in $Al_{80}Ni_{20}$ melts: Simulation and experiment. Phys Rev B, 2007, 75: 174304
- 22 Wang L, Wang Y Q, Peng C X, et al. Medium-range structural order in liquid $Ni_{20}Al_{80}$ alloy: Experimental and molecular dynamics studies. Phys Lett A, 2006, 350(5-6): 405–409
- 23 Miracle D B, Senkov O N. A geometric model for atomic configurations in amorphous Al alloys. J Non-Cryst Solid, 2003, 319: 174– 101
- 24 Sheng H W, Cheng Y Q, Lee P L, et al. Atomic packing in multicomponent aluminum-based metallic glasses. Acta Mater, 2008, 56: 6264–6272
- 25 Li G Q, Borisenko K B, Chen Y X. Local structure variations in

- Al₈₉La₆Ni₅ metallic glass. Acta Mater, 2009, 57(3): 804-811
- 26 Bernal J D. A geometrical approach to the structure of liquids. Nature, 1959, 183(4655): 141–147
- 27 Miracle B D. A structural model for metallic glasses. Nat Mater, 2004, 3(10): 697–702
- 28 Sheng H W, Luo W K, Alamgir F M, et al. Atomic packing and short-to-medium-range order in metallic glasses. Nature, 2006, 439: 419–425
- 29 Li Y, Guo Q, Kalb J. A, et al. Matching glass-forming ability with the density of the amorphous phase. Science, 2008, 322: 1816–1819
- 30 Car R, Parrinello M. Unified approach for molecular dynamics and density-functional theory. Phys Rev Lett, 1985, 55(22): 2471–2474
- 31 Kresse G, Furthmüller J. Efficiency of ab-initio total energy calculations for metals and semiconductors using a plane-wave basis set. Comput Mater Sci, 1996, 6(1): 15–50
- 32 Kresse G, Furthmüller J. Efficient iterative schemes for ab initio total-energy calculations using a plane-wave basis set. Phys Rev B, 1996, 54(16): 11169–11186
- 33 Blöchl P E. Projector augmented-wave method. Phys Rev B, 1994, 50(24): 17953–17979
- 34 Kresse G, Joubert D. From ultrasoft pseudopotentials to the projector augmented-wave method. Phys Rev B, 1999, 59(3): 1758–1775
- Wang Y, Perdew J P. Correlation hole of the spin-polarized electron gas, with exact small-wave-vector and high-density scaling. Phys Rev B, 1991, 44(24): 13298–13307
- 36 Nose S. A unified formulation of the constant temperature molecular dynamics methods. J Chem Phys, 1984, 81(1): 511–519
- 37 Verlet L. Computer "experiments" on classical fluids. I. Thermodynamical properties of Lennard-Jones molecules. Phys Rev, 1967, 159(1): 98–103
- 38 Shimoli M. Liquid Metals. Washington: Academic Press, 1977
- 39 Mattern N, Kuʻhn U, Hermann H, et al. Short-range order of $Zr_{62*x}Ti_xAl_{10}Cu_{20}Ni_8$ bulk metallic glasses. Acta Mater, 2002, 50: 305-314
- 40 Allen M P, Tildesley D J. Computer Simulation of Liquids. Oxford: Oxford University Press, 1989
- 41 Maret M, Pomme T, Pasturel A. Structure of liquid Al₈₀Ni₂₀ alloy. Phys Rev B, 1990, 42(3): 1598–1604
- 42 Finney J L. Random packings and the structure of simple liquids: The geometry of random close packing. Proc R Soc Lond A, 1970, 319(1539): 479–493
- 43 Nelson D R. Order, frustration, and defects in liquids and glasses. Phys Rev B, 1983, 28: 5515–5535
- 44 Bernal J D. Geometry of the structure of monatomic liquids. Nature, 1960, 185(4707): 68–70
- 45 Zalewski W, Antonowicz J, Bacewicz R. Local atomic order in Al-based metallic glasses studied using XAFS method. J Alloy Compd, 2009, 468: 40–46
- 46 Hsieh H Y, Toby B H, He Y. Atomic structure of amorphous Al₉₀Fe_xCe_{10-x}. J Mater Res, 1990, 5(12): 2807–2812
- 47 Cowley J M. An approximate theory of order in alloys. Phys Rev, 1950, 77(5): 669–675
- 48 Widom M, Lehyani A I, Moriarty J A. First-principles interatomic potentials for transition-metal aluminides. Phys Rev B, 2000, 62(6): 3648–3657
- 49 Mukherjee S, Schroers J, Zhou Z. Viscosity and specific volume of bulk metallic glass-forming alloys and their correlation with glass forming ability. Acta Mater, 2004, 52(12): 3689–3695
- 50 Yokoyama Y, Ishikawa T, Okada J T. Volume and viscosity of Zr-Cu-Al glass-forming liquid alloys. J Non-Cryst Solid, 2009, 355: 317–322